JACS
JOURNAL OF THE AMERICAN CHEMICAL SOCIETY
Article
Cite This: J. Am. Chem. Soc. 2020, 142, 884−893
pubs.acs.org/JACS

Unraveling the Mechanism of Catalytic Water Oxidation via *de Novo* Synthesis of Reactive Intermediate

Alireza Karbakhsh Ravari, Guibo Zhu, Roman Ezhov, Yuliana Pineda-Galvan, Allison Page, Whitney Weinschenk, Lifen Yan, and Yulia Pushkar*

Department of Physics, Purdue University, 525 Northwestern, West Lafayette, Indiana 47907, United States

Supporting Information

ABSTRACT: Artificial photosynthesis could promise abundant, carbon-neutral energy, but implementation is currently limited by a lack of control over the multi-electron catalysis of water oxidation. Discoveries of the most active catalysts still rely heavily on serendipity. $[Ru(tpy)(bpy)(H_2O)]^{2+}$ (**1**; bpy = 2,2′-bipyridine, tpy = 2,2′;6′,2″-terpyridine) is representative of the largest known class of water oxidation catalysts. We undertook an extensive spectroscopic analysis of the prototypical **1** water oxidation catalyst and its fastest known analog $[Ru(EtO\text{-}tpy)(bpy)(H_2O)]^{2+}$ (**2**), capable of 10 times faster water oxidation, to investigate the mechanism of action and factors controlling catalytic activity. EPR and resonance Raman spectroscopy did not detect the proposed $[Ru^{V}{=}O]$ intermediate in **1** and **2** but indicated the possible formation of N-oxides. A lag phase was observed prior to O_2 evolution, suggesting catalyst modification before the onset of catalysis. The reactive intermediate $[Ru(tpy)(bpy\text{-}NO)(H_2O)]^{2+}$ (**1-NO**; bpy-NO = 2,2′-bipyridine-N-oxide) proposed by combined spectroscopic and DFT analysis was *de novo* synthesized and demonstrated 100-fold greater catalytic activity than **1**. Thus, *in situ* transient formation of small amounts of the Ru complex with N-oxide ligands can significantly activate single-site Ru-based catalysts. Furthermore, the rate of O_2 evolution was found to correlate with the redox potential of the ligand. This observation might assist with rational design of new catalysts.

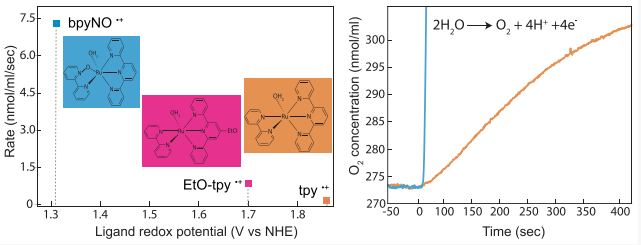

INTRODUCTION

The growing amount of greenhouse gases, especially CO_2, in the atmosphere has been connected with climate change and higher incidence of severe weather events. A significant increase in the generation of renewable, CO_2-neutral energy is required to satisfy growing energy demands worldwide.[1] The creation of a man-made device mimicking the light-induced water splitting which occurs during natural photosynthesis[2−6] would enable solar energy-to-fuel conversion schemes.[7−10] Intermittent electricity from solar and wind can potentially be converted into fuels via water splitting, but such processes are currently expensive. Development of artificial photosynthesis as well as the optimization of modern electrolyzers hinges on the understanding water oxidation mechanisms in both the natural oxygen-evolving complex of Photosystem II[2−5,11,12] and man-made catalysts.[13,14]

O−O bond formation can proceed via two main mechanisms: water nucleophilic attack (WNA) and radical coupling (RC).

$$\text{WNA:}\quad [M{=}O]^{n+} + H_2O \rightarrow [M{-}OOH]^{(n-1)+} + H^+$$

$$\text{RC:}\quad 2[M{=}O]^{n+} \rightarrow [M{-}O{-}O{-}M]^{2n+}$$

Both mechanisms require formation of highly oxidized metal-oxo (M=O) species which are typically achieved from M−H_2O via proton-coupled electron transfer (PCET). Molecular catalysts for water oxidation provide a convenient system for detailed mechanistic analysis.[15] While such catalysts have been reported for multiple metal ions, Ru-based complexes remain the most stable and the most studied.[7−10,16−18] Mechanistic analysis with spectroscopic identification of reactive intermediates is available for the first discovered molecular water oxidation catalyst, blue dimer (BD),[19] where the formation of the $[Ru^{IV},Ru^{V}{=}O]$ intermediate was confirmed by X-ray spectroscopy and electron paramagnetic resonance (EPR; Figure 1A).[20,21] $[Ru^{IV},Ru^{V}{=}O]$ is expected to react with water via WNA. However, the resulting peroxo intermediates have not yet been unambiguously identified.[22] $[(bpy)_2Ru^{V}{=}O,OH]^{2+}$ was identified by EPR and can react via both WNA and RC.[23,24] Its high activity, however, subsides to quick deactivation via dimer formation.[24]

Introduction of the negatively charged bda (H_2bda = 2,2′-bipyridine-6,6′-dicarboxylic acid) ligand resulted in a family of fast $Ru^{II}(L)_2$(bda) catalysts (Figure 1B).[25,26] These react quickly in solution via RC, as evidenced by a rate of O_2 evolution that is second order on the catalyst. Immobilization of the $Ru^{II}(L)_2$(bda) complex on the electrode surface allowed the first spectroscopic characterization of the key 7-coordinate $[Ru^{V}{=}O(L)_2(bda)]^{+}$ intermediate.[16] The bda family of

Received: September 23, 2019
Published: December 22, 2019

DOI: 10.1021/jacs.9b10265
J. Am. Chem. Soc. 2020, 142, 884−893

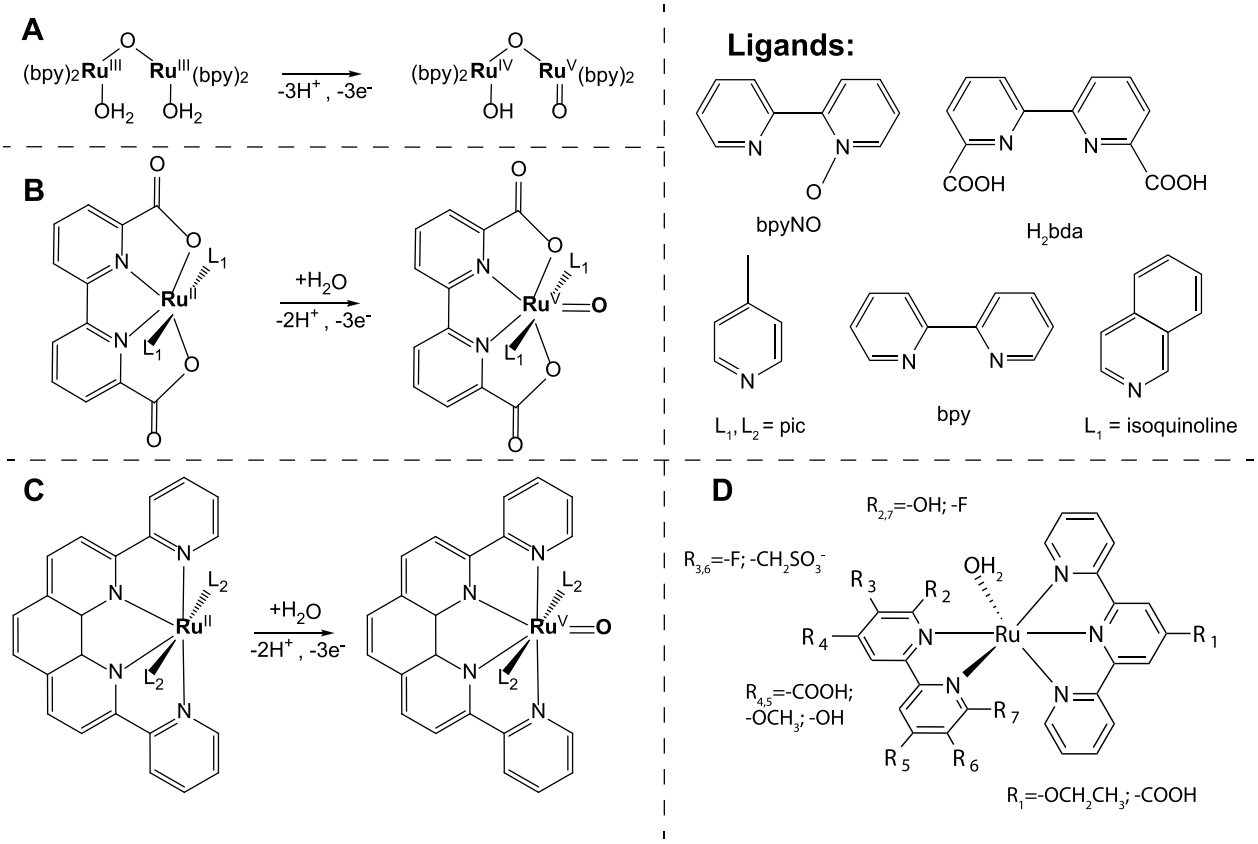

Figure 1. Activated Ru-based species capable of O−O bond formation and oxygen atom transfer. (A) Formation of the activated $[Ru^{IV},Ru^{V}{=}O]$ intermediate in the blue dimer is achieved via PCET. (B) The $Ru^{II}(L)_2(bda)$ class of WOCs forms 7-coordinate $Ru^{V}{=}O$ intermediates via coordination sphere expansion and PCET. Catalysts with a variety of axial ligands were investigated; two typical axial ligands (L_1) are shown. (C) The 7-coordinate $[Ru^{V}{=}O(L)_2(dpp)]^{3+}$ intermediate with neutral dpp ligand is stable in solutions on a minute time scale due to ligand protection of the $Ru^{V}{=}O$ fragment. Activation occurs via oxygen atom transfer with formation of dpp-N-oxides. (D) Overview of ligand modifications in the $[Ru^{II}(bpy)(tpy)(H_2O)]^{2+}$ family of catalysts. It has been shown that ethoxy (EtO−) and methoxy (MeO−) substituents increase the rate of O_2 evolution.

catalysts currently demonstrate the highest rate of water oxidation in acidic solutions. However, surface immobilization significantly lowers the catalytic rate, as it disrupts the RC pathway. Neutral polypyridine ligands can also support the formation of a 7-coordinate $[Ru^{V}{=}O(L)_2(dpp)]^{3+}$ intermediate under oxidizing conditions (Figure 1C). The increased lifetime of this species was attributed to the protective effect of the ligand environment.[27]

Despite recent spectroscopic advances, there remains a large class of Ru complexes with currently unexplained mechanisms of action. These complexes utilize neutral polypyridine ligands and single water as a direct ligand to Ru (Figure 1D). In this study, we focus on the basic catalyst family of $[Ru^{II}(bpy)(tpy)(H_2O)]^{2+}$ (**1**; tpy = 2,2′;6′,2″-terpyridine, bpy = 2,2′-bipyridine), the framework of which was used extensively for ligand modification to uncover structure−activity relationships (Figure 1D). The following ligand modifications were reported: $R_{2,4}$ = −OMe, −COOH;[28] $R_{2,7}$ = −OH, $R_{4,5}$ = −OH, $R_{2,4}$ = −OMe;[29] $R_{2,7}$ = −F, $R_{3,6}$ = −F;[30] $R_{3,6}$ = $-CH_2SO_3^-$;[31] R_1 = −OEt, −OMe, −Me, −Cl.[32] Extensive studies have shown that introduction of the ethoxy (EtO−) and methoxy (MeO−) substituents on tpy or bpy ligands increases the rate of O_2 evolution by as much as a factor of 10. Other modifications were moderately activating or moderately deactivating. Faster O_2 evolution was attributed to the decrease in redox potential of the $[Ru^{V}{=}O(bpy)(EtO\text{-}tpy)]^{3+}$ formation.[32,33] Catalysts of this type are also widely tested for incorporation in functional assemblies but, so far, with limited success.[34,35]

Our quest for an alternative mechanism was driven by an apparent controversy in the field of catalytic water oxidation. While multiple PCET accessible $Ru^{V}{=}O$ (S = 1/2) intermediates critical for O−O bond formation were detected (Figure 1A−C),[16,20,21,24,27] $[(5N\text{-ligands})Ru^{V}{=}O]^{3+}$ intermediates[28,36,37] and products of its reaction with water have never been observed (blue path in Figure 2).[17,18] Here, catalyst activation proceeds via PCET to $Ru^{IV}{=}O$ steady-state species characterized *in situ* by X-ray absorption spectroscopy (XAS) and resonance Raman (RR) spectroscopy (green box, Figure 2)[15,17,18,38] However, $Ru^{IV}{=}O$ does not have enough energy to react with water via WNA or RC. The PCET channel to form a $Ru^{V}{=}O$ state is not available, and direct oxidation (without PCET) appears to be thermodynamically prohibitive (see Figure 2, inset).[17,18] For Ru complexes with neutral polypyridine ligands, WNA on a $Ru^{V}{=}O$ species to form an O−O bond adds a second (~0.6−1.1 eV) barrier.[39−44] In total, two significant, consecutive activation barriers must be overcome first to generate the $Ru^{V}{=}O$ and then for its reaction with water. Some studies proposed direct involvement of Ce^{IV} (via hydroxo-Ce^{IV} fragment) to facilitate O−O bond formation[28,45] and to bind with Ru complexes.[22,28] While we recently characterized a $Mn^{IV}{=}O{\cdots}Ce^{IV}$ adduct,[46] our earlier

DOI: 10.1021/jacs.9b10265
J. Am. Chem. Soc. 2020, 142, 884−893

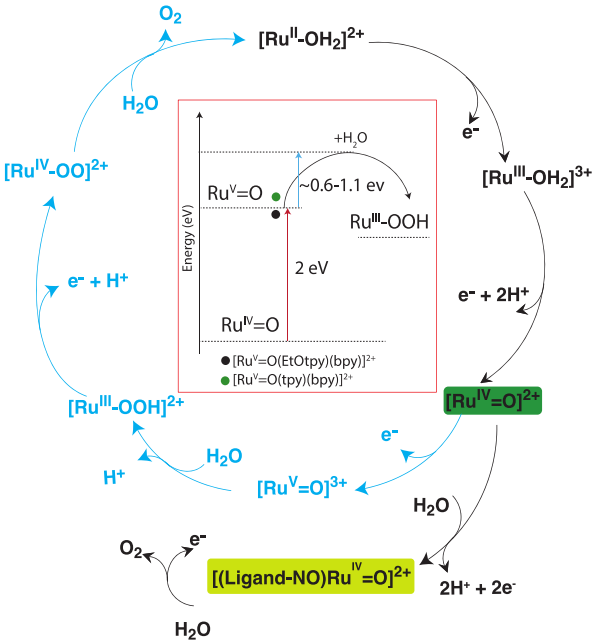

Figure 2. Catalytic cycle of $[Ru^{II}(5N\text{-ligands})H_2O]^{2+}$ family of catalysts (Figure 1D). There is ~95% $[Ru^{IV}{=}O(bpy)(tpy)]^{2+}$ in the catalytic steady state. Involvement of the $Ru^{V}{=}O$ and proposed O—O bond formation via WNA (blue arrows) currently lacks experimental confirmation. For Ru complexes with neutral polypyridine ligands, this pathway has a high total barrier to O—O bond formation, as two significant, consecutive activation barriers must be overcome: first to generate the $Ru^{V}{=}O$ and second for its reaction with water (middle inset). The lag phase in the onset of O_2 evolution indicates an additional step of catalyst activation (yellow box).

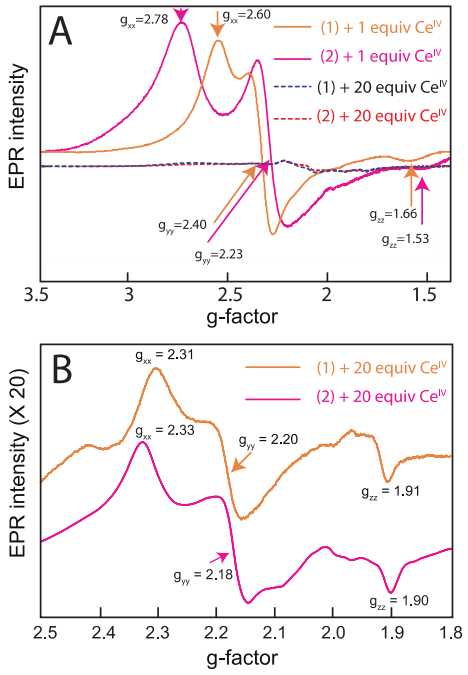

Figure 3. (A) EPR spectra of **1** (orange) and **2** (magenta) in 0.1 M HNO_3 after addition of 1 equiv of Ce^{IV} (solid lines) and after addition of 20 equiv of Ce^{IV} (dash lines). (B) Zoom (×20) into low-intensity EPR signals from solutions generated by adding 20 equiv of Ce^{IV} in 0.1 M HNO_3 to **1** (orange) and to **2** (magenta). All samples were frozen within 30 s.

extended X-ray absorption fine structure (EXAFS) study of Ru-based catalysts did not reveal structural signatures of the $Ru^{IV}{=}O{\cdots}Ce^{IV}$ or other adducts with Ce^{IV}.

Thus, there is a need for a new hypothesis on how such molecular catalysts can be transformed to achieve water oxidation reaction. All these catalysts commonly use polypyridine ligands. Recently, we have shown that both 6-coordinate $Ru^{IV}{=}O$ and 7-coordinate $Ru^{V}{=}O$ can efficiently transfer oxygen to nitrogens in polypyridine ligands, with the formation of N-oxides.[17,27,47] Computationally, the $[Ru^{IV}{=}O(tpy)(L)]^{2+}$ was shown to convert to intermediates with coordinated N-oxide.[48]

Here, using a combination of *in situ* spectroscopy and *de novo* synthesis of the reactive intermediate, we were able to establish that formation of the complex with an N-oxide ligand has a key activating role for the $[(5N\text{-ligands})Ru(H_2O)]^{2+}$ class of catalysts. This discovery resulted from detailed spectroscopic analysis and identification of transient reactive intermediates. Direct synthesis of the reactive intermediate $[Ru^{II}(tpy)(bpy\text{-}NO)(H_2O)]^{2+}$ (**1-NO**) validated a multitude of *in situ* spectroscopic observations and computational predictions. Overall, single-atom modification of the ligand resulted in a 100-fold increase in catalytic activity.

RESULTS AND DISCUSSION

1. Spectroscopic Characterization of Water Oxidation Using $[Ru^{II}(bpy)(tpy)(H_2O)]^{2+}$ (1) and $[Ru(bpy)(EtO\text{-}tpy)(H_2O)]^{2+}$ (2). Upon addition of 1 equiv of Ce^{IV} to **1** and **2**, Ru^{III} (S = 1/2) forms with g_{xx} = 2.60, g_{yy} = 2.4, and g_{zz} = 1.66 in **1** and g_{xx} = 2.78, g_{yy} = 2.33, and g_{zz} = 1.53 in **2** (Figure 3A). Such Ru^{III} (S = 1/2) EPR signals are well known.[17,18,38,49] Under catalytic conditions, modeled here by adding 20 equiv of Ce^{IV}, the majority of the **1** and **2** is in the EPR-silent $[Ru^{IV}{=}O]$ state (S = 1) (see decrease in EPR intensity in Figure 3A). Residual (~5%) EPR signals in Figure 3B (g_{xx} = 2.31, g_{yy} = 2.20, and g_{zz} = 1.91 for **1**[18,38] and g_{xx} = 2.33, g_{yy} = 2.18, and g_{zz} = 1.90 for **2**) do not match expected g-factors of the $Ru^{V}{=}O$ (S = 1/2) species (Table S1).[16,23,24,27,50] Reported $Ru^{V}{=}O$ g-factors show g_{xx} ranging from 2.05 to 2.08, and g_{yy} from 1.98 to 2.01, and g_{zz} from 1.85 to 1.91 (Table S1). For **1** using a combination of EPR and XAS, we demonstrated earlier that 95% of the Ru complex in the catalytic steady state is in the form of $[Ru^{IV}{=}O(bpy)(tpy)]^{2+}$.[18] According to literature reports, the $Ru^{V}{=}O$ state should be more accessible in $[Ru(bpy)(EtO\text{-}tpy)(H_2O)]^{2+}$ (**2**).[32,33] However, similar to **1**, a low-intensity EPR signal with g_{xx} = 2.33, g_{yy} = 2.18, and g_{zz} = 1.90 is detected here instead of the expected EPR associated with $[Ru^{V}{=}O(bpy)(EtO\text{-}tpy)]^{3+}$. The EPR signals in Figure 3B form quickly and are not sensitive to the nature of the acid, ruling out their origin as anation products. Since our 2014 report,[18] EPR spectra with similar g-tensors were found for Ru complexes $[Ru^{III}(NPM\text{-}NO)(4\text{-}pic)_2(H_2O)]^{3+}$ and $[Ru^{III}(NPM\text{-}NO,NO)(4\text{-}pic)_2]^{3+}$ (where NPM = 4-*tert*-butyl-2,6-di(1′,8′-naphthyrid-2′-yl)-pyridine and pic = 4-picoline) (g_{xx} = 2.30, g_{yy} = 2.18, g_{yy} = 1.83)[17] and in the $[Ru^{III}(pic)_2(dpp\text{-}NO)]^{3+}$ (g_{xx} = 2.39, g_{yy} = 2.16, g_{zz} = 1.86) and $[Ru^{III}(pic)_2(dpp\text{-}NO,NO)]^{3+}$ (g_{xx} = 2.23, g_{yy} = 2.16, g_{zz} = 1.92) catalytic intermediates, which all featured the N-oxide ligands.[27]

Resonance Raman (RR) with $^{16}O/^{18}O$ isotope labeling is particularly helpful with identification of key Ru=O, Ru—O, and possibly O—O bonds (Figure 4, Figure S1). In **1** and **2** oxidized with 20 equiv of Ce^{IV} in 0.1 M $HNO_3/H_2{}^{16}O$ or

DOI: 10.1021/jacs.9b10265
J. Am. Chem. Soc. 2020, 142, 884−893

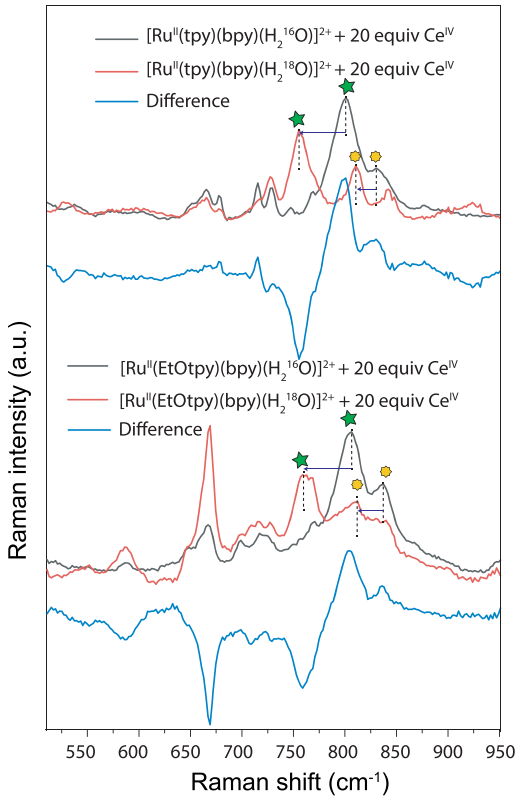

Figure 4. Selected frequency range of resonance Raman spectra (532 nm) of 1 mM solutions of **1** and **2** in 0.1 M HNO_3 mixed with 20 equiv of Ce^{IV} (1 min after oxidation) in $H_2{}^{16}O$ and $H_2{}^{18}O$ (Figure S1, Table S2). Two isotope-sensitive vibrations were assigned to Ru^{IV}=O (~800 cm^{-1}) and Ru—O—N (~830 cm^{-1}).

$H_2{}^{18}O$, the major band at 800 cm^{-1} undergoes a −45 cm^{-1} shift. This band was previously assigned to Ru^{IV}=O and similar isotope shifts were reported.[17,51] Interestingly, the 800 cm^{-1} band was accompanied by the $^{16}O/^{18}O$ isotope-sensitive band (−20 cm^{-1}) at ~831 cm^{-1} detected previously[52] and assigned to $[(tpy)Ru^{VI}{=}O,{=}O,OH]^+$. The RR spectrum of the $[(tpy)Ru^{VI}{=}O,{=}O,OH]^+$, prepared as a reference compound, showed an isotope shift of −44 cm^{-1} for its symmetric Ru^{VI}=O,=O vibration at 833 cm^{-1} (Figure S2). While a −44 cm^{-1} shift is consistent with the Ru^{VI}=O nature of the bond, a −20 cm^{-1} shift is more appropriate for a single Ru−O bond. To the best of our knowledge, only the Ru−O−N vibration of N-oxides coordinated to Ru is known to be at ~830 cm^{-1}.[27,53]

We also obtained a lag phase (delay in O_2 evolution after addition of Ce^{IV} oxidant) on the order of 2−20 s for 0.1 mM solution of **2** and 40−100 s for the 1.0 mM solution of less active **1** (Table S3, Figure S3). The lag phase is shorter for more active **2**. An increase in Ce^{IV} concentration results in the shorter lag phase. From this result, we believe both complexes undergo an additional activation step, in agreement with earlier reports[43] for **1**. The classical mechanism of O−O bond formation via water nucleophilic attack (Figure 2) is inconsistent with experimental observations of the lag phase. An activation period on the order of minutes was observed in Ru-based water oxidation catalysts with quaterpyridine ligands, and it was attributed to qpy-N,N‴-dioxide formation as a key step in catalyst activation.[27,47]

Dimer formation was noted for **1** and its analogs under prolonged oxidation (Figure S4). It has been reported that prolonged bulk electrolysis or prolonged oxidation (several days to 1 week) with an excess of Ce^{IV} of **1** and its analogs might result in dimerization of this complex with formation of more stable but less active $[(tpy)(bpy)Ru^{IV}\text{-}O\text{-}Ru^{IV}(tpy){=}O(OH)]^{4+}$.[54,55] The analog with bpyms = 2,2′-bipyridine-5,5′-bis(methanesulfonate) delivered crystals with $[(tpy)(bpyms)Ru^{III}\text{-}O\text{-}Ru^{III}(tpy)(bpyms)]^{4+}$ dimer after 3 weeks with Ce^{IV}.[31] Formation of the bpy N-oxide and its consecutive de-coordination might be responsible for the reported $[(tpy)(bpy)Ru^{IV}\text{-}O\text{-}Ru^{IV}(tpy){=}O(OH)]^{4+}$ dimer formation. We demonstrated that catalysts' deactivation via dimerization can be effectively prevented for catalysts immobilized in metal−organic frameworks.[34,51] XRD analysis of late dimeric products delivered limited information on *in situ* processes at early times and, in particular, on catalysts' activation at the onset of catalytic current. Formation of free bpy-NO was noted under catalytic conditions.[28] Thus, we reasoned that while dimer formation cannot account for the lag phase, ligand N-oxide formation can happen quickly at the Ru^{IV}=O level (~95% in catalytic steady state)[18] and result in catalyst activation. This hypothesis is tested below via *de novo* synthesis of the proposed reactive intermediate.

2. *De Novo* Synthesis of $[Ru(tpy)(bpy\text{-}NO)(H_2O)]^{2+}$ (1-NO). The catalytic intermediate $[Ru(tpy)(bpy\text{-}NO)(H_2O)]^{2+}$ (**1-NO**) was prepared, and its performance in O_2 evolution was investigated (Figure 5). To the best of our knowledge, few Ru complexes with N-oxide ligands have been described.[47,53,56,57] Earlier we[53] and others[56] were able to synthesize $[Ru^{II}(bpy)_2(bpy\text{-}NO)]^{2+}$. However, this compound is extremely light sensitive. [Ru(tpy)(bpy-NO)Cl]Cl was prepared using a procedure similar to the synthesis of $[Ru^{II}(bpy)(tpy)Cl]Cl$ with some modifications.[58] All preparations were handled in the dark due to its unknown properties. **1-NO** turned out to be a reactive compound with a tendency to convert to **1** under the conditions of the synthesis. Regardless of the precautions and explored alternative synthetic routes, mixtures of $(tpy)(bpy)RuCl_2$ and $(tpy)(bpy\text{-}NO)RuCl_2$ were obtained. Facile conversion of $[Ru(tpy)(bpy\text{-}NO)(X)]$ to $[Ru(tpy)(bpy)(X)]$ happens under the conditions of the synthesis, in stark contrast to $[Ru^{II}(bpy)_2(bpy\text{-}NO)]^{2+}$, which was prepared with good yields.[53] We attributed this dramatic difference to the much higher reactivity of $[(tpy)(bpy\text{-}NO)Ru(X)]^{2+}$. We noted that the decrease of the water content from 25% to 5% in the reaction mixture helps to increase the **1-NO** content. We also noted that in $[(tpy)(bpy\text{-}NO)RuCl]^+$ Cl ligand exchanges faster than in **1**. Thus, we can speculate that the presence of the liable Ru-Cl and/or Ru-H_2O ligand is responsible for the conversion of **1-NO** to **1**, especially when heated.

Despite the mixed content, such catalyst preparations already demonstrated a 10-fold increase in the rate of catalytic water oxidation using Ce^{IV} (Figure S5). Separation on silica gel allowed us to purify *trans-* and *cis*-**1-NO**. UV−vis and FTIR data (Figure 5A,B) show distinct spectroscopic signatures of **1-NO**, which include a purple color and ~830 cm^{-1} vibration also noted in the $[Ru^{II}(bpy)_2(bpy\text{-}NO)]^{2+}$ complex.[53] *cis*-**1-NO** demonstrated high catalytic activity (Figure 5C,D). To the best of our knowledge, this is the highest O_2 evolution activity reported for a single-site Ru-based catalyst in acid and with first-order rate dependence on the catalyst complex. Note that some faster catalysts are accessible via a radical coupling

DOI: 10.1021/jacs.9b10265
J. Am. Chem. Soc. 2020, 142, 884−893

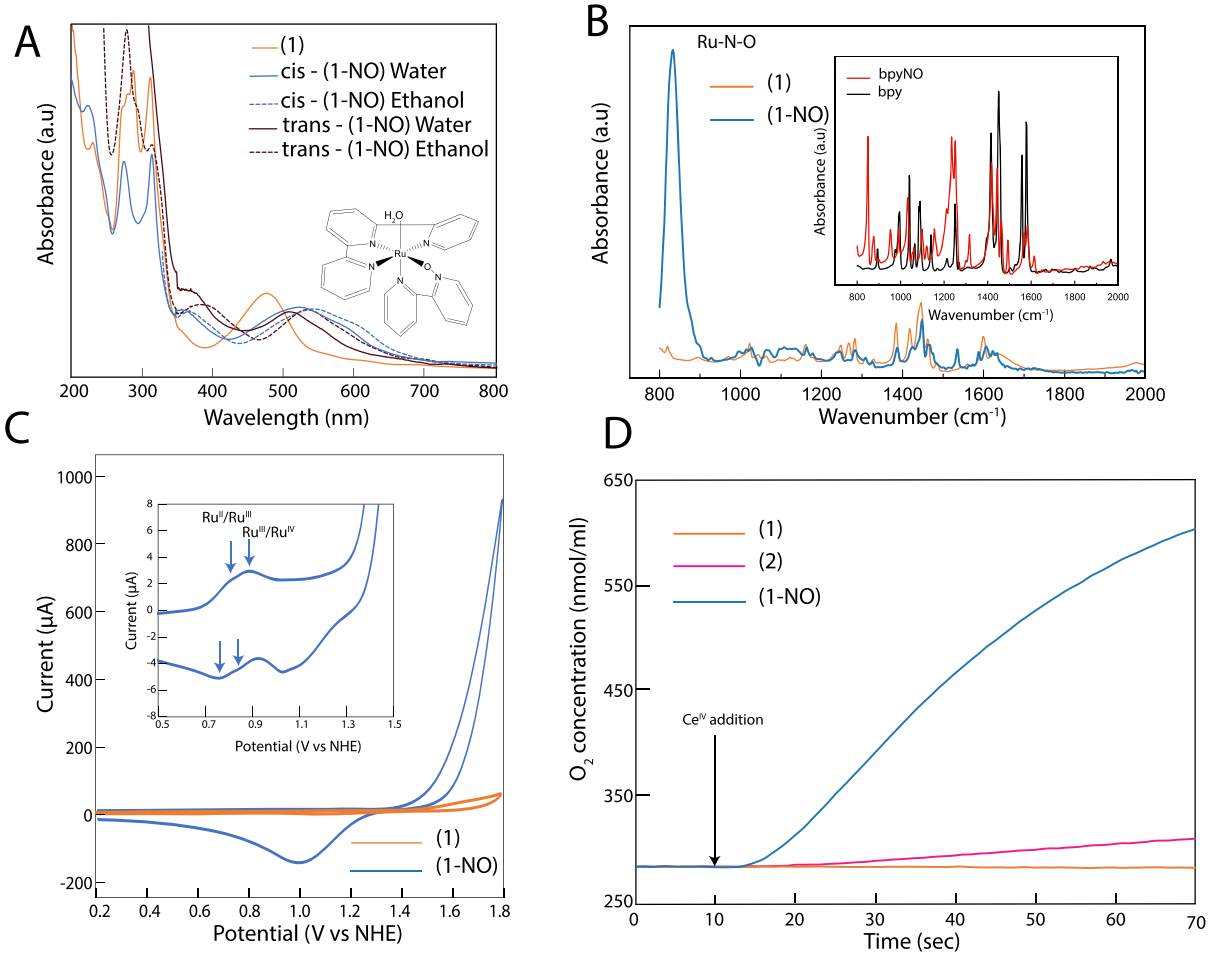

Figure 5. Spectroscopic and catalytic properties of the $[Ru(tpy)(bpy\text{-}NO)(H_2O)]^{2+}$ (**1-NO**) intermediate. (A) UV−vis absorption of **1**, *trans*-**1-NO**, and *cis*-**1-NO**. Ethanol solutions contain *trans*- and *cis*-$[Ru(tpy)(bpy\text{-}NO)Cl]^{+}$ correspondingly. In $[Ru(tpy)(bpy\text{-}NO)Cl]^{+}$, Cl undergoes fast exchange in water. (B) FTIR of **1** and **1-NO** powders. Inset shows FTIR of pure ligands. (C) Cyclic voltammetry of 0.5 mM **1** and *cis*-**1-NO** in 0.1 M HNO_3, scan rate 0.1 V/s. Inset shows the Ru^{II}/Ru^{III} and Ru^{III}/Ru^{IV} couples. (D) Oxygen evolution of **1**, **2**, and *cis*-**1-NO** prepared by mixing 1 mL of a 0.2 mM solution and 40 equiv of Ce^{IV} in 0.1 M HNO_3.

mechanism,[25,59] but these cannot currently be integrated into devices, as at pH 1 their activity decreases upon immobilization. The *trans*-**1-NO** isomer forms in unpractically small amounts and was not investigated beyond UV−vis and NMR characterization.

The electrochemical properties of *cis*-**1-NO** were investigated by cyclic voltammetry (Figure 5C). Redox events at ∼0.8−0.9 V vs NHE are likely the oxidation of the Ru^{II} to Ru^{III} and later to Ru^{IV} predicted by DFT at ∼1 V (Table 1, Table S7). The oonset of catalytic current at ∼1.4 V is the lowest known for Ru-based complexes outside the Ru-bda family.[25] The overall high catalytic activity of the *cis* **1-NO** intermediate shows that the formation of such or analogous tpy-NO intermediates at a level of few percent might be fully responsible for all observed catalytic activity of $[(tpy)(bpy)\text{-}Ru(H_2O)]^{2+}$ and its large family of analogs.

3. DFT Analysis of Catalytic Mechanism. DFT was used here to support the analysis of redox properties, spectroscopic signatures, and chemical reactivity of Ru-based catalysts (Table 1, Tables S4−S7). Latimer−Frost diagrams for a variety of possible intermediates and reactivity pathways give a better understanding of the feasibility of catalysts' activation via formation of N-oxide ligands and their further reactivity (Figures S6−S9). Calculations for the redox potentials of **1**, **1-NO**, and **2** (Table 1) agree well with the literature reports[32,33] and measurements for **1-NO**.

The redox potential for the $[Ru^{V}{=}O(bpy)(EtO\text{-}tpy)]^{3+}$ formation was found to be ∼1.98 V, which is slightly lower than ∼2.15 V computed for $[Ru^{V}{=}O(bpy)(tpy)]^{3+}$ and ∼2.12 for $[Ru^{V}{=}O(bpy\text{-}NO)(tpy)]^{3+}$ (Table 1). Neither potential is accessible to the Ce^{IV} oxidant (∼1.7 V).

We also analyzed the reactivity of $Ru^{IV}{=}O$ in **1** and **2** in the oxygen atom transfer to bpy, tpy, and EtO-tpy ligands with the formation of ligand-N-oxides (Table 1). The free energies in both paths are small (∼0.1 eV), and transfers to tpy and EtO-tpy are more favorable compared to the transfer to bpy. Preliminary computational analysis by another group[48] has shown similar results. Both bpy-NO and tpy-NO ligand modifications could exist under the reaction conditions.

It has long been noted that the redox potentials of the Ru complexes correlate poorly with catalytic activity in water oxidation.[59] With three molecularly highly similar catalysts spanning 2 orders of magnitude in catalytic activity, we searched for a molecular property which correlates with O_2 evolution rates. Formation of the $Ru^{V}{=}O$ state is considered key to both pathways of O−O bond formation via radical

DOI: 10.1021/jacs.9b10265
J. Am. Chem. Soc. 2020, 142, 884−893

Table 1. Key Thermodynamic Parameters Computed Using DFT

reaction[a]	ΔG^0/eV	E^0/V[b]
Redox Reactions		
(**2**)$[Ru^{III}(EtO\text{-}tpy)(bpy)(H_2O)]^{3+}/2H_2O + e^- \rightarrow [Ru^{II}(EtO\text{-}tpy)(bpy)(H_2O)]_{2+}/2H_2O$		+1.03 (+0.98 [32])
(**2**)$[Ru^{IV}{=}O(EtO\text{-}tpy)(bpy)]^{2+}/2H_2O + e^- + 2H^+ \rightarrow [Ru^{III}(EtO\text{-}tpy)(bpy)(H_2O)]^{3+}/2H_2O$		+1.14 (+1.24 [32])
(**1**)$[Ru^{III}(tpy)(bpy)(H_2O)]^{3+}/2H_2O + e^- \rightarrow [Ru^{II}(tpy)(bpy)(H_2O)]^{2+}/2H_2O$		+1.10 (+1.04 [28])
(**1**)$[Ru^{IV}{=}O(tpy)(bpy)]^{2+}/2H_2O + e^- + 2H^+ \rightarrow [Ru^{III}(tpy)(bpy)(H_2O)]^{3+}/2H_2O$		+1.12 (+1.23 [28])
(**1-NO**)$[Ru^{III}(tpy)(bpy\text{-}NO)(H_2O)]^{3+}/2H_2O + e^- \rightarrow [Ru^{II}(tpy)(bpy\text{-}NO)(H_2O)]^{2+}/2H_2O$		+1.01 (+0.82)
(**1-NO**)$[Ru^{IV}{=}O(tpy)(bpy\text{-}NO)]^{2+}/2H_2O + e^- + 2H^+ \rightarrow [Ru^{III}(tpy)(bpy\text{-}NO)(H_2O)]^{3+}/2H_2O$		+0.89 (+0.86)
$Ru^V{=}O$ Formation		
(**2**)$[Ru^{V}{=}O(EtO\text{-}tpy)(bpy)]^{3+}/2H_2O + e^- \rightarrow [Ru^{IV}{=}O(EtO\text{-}tpy)(bpy)]^{2+}/2H_2O$		+1.98
(**1**)$[Ru^{V}{=}O(tpy)(bpy)]^{3+}/2H_2O + e^- \rightarrow [Ru^{IV}{=}O(tpy)(bpy)]^{2+}/2H_2O$		+2.15
(**1-NO**)$[Ru^{V}{=}O(tpy)(bpy\text{-}NO)]^{3+}/H_2O + e^- \rightarrow [Ru^{IV}{=}O(tpy)(bpy\text{-}NO)]^{2+}/H_2O$		+2.12
$Ru^{IV}{=}O(Ligand^{\bullet+})$ Formation		
(**1-NO**)$[Ru^{IV}{=}O(tpy)(bpy\text{-}NO^{\bullet+}{}_{out})(OH)]^{2+} + e^- + H^+ \rightarrow [Ru^{IV}{=}O(tpy)(bpy\text{-}NO_{out})(H_2O)]^{2+}$		+1.51
Oxygen Atom Transfer to Ligand with Formation of N-Oxide		
(**2**)$[Ru^{IV}{=}O(EtO\text{-}tpy)(bpy)]^{2+}/2H_2O \rightarrow [Ru^{II}(EtO\text{-}tpy\text{-}NO)(bpy)(H_2O)]^{2+}/H_2O$	−0.09	
(**2**)$[Ru^{IV}{=}O(EtO\text{-}tpy)(bpy)]^{2+}/2H_2O \rightarrow [Ru^{II}(EtO\text{-}tpy)(bpy\text{-}NO)(H_2O)]^{2+}/H_2O$	+0.14	
(**1**)$[Ru^{IV}{=}O(tpy)(bpy)]^{2+}/2H_2O \rightarrow [Ru^{II}(tpy\text{-}NO)(bpy)(H_2O)]^{2+}/H_2O$	−0.13	
(**1**)$[Ru^{IV}{=}O(tpy)(bpy)]^{2+}/2H_2O \rightarrow [Ru^{II}(tpy)(bpy\text{-}NO)(H_2O)]^{2+} + H_2O$	+0.09	
Oxidation of the Ligand with Formation of Cation Radical		
$tpy^{\bullet+} + e^- \rightarrow tpy$		+1.86
$EtO\text{-}tpy^{\bullet+} + e^- \rightarrow EtO\text{-}tpy$		+1.70
$bpyNO^{\bullet+} + e^- \rightarrow bpyNO$		+1.31

[a] $/H_2O$ denotes explicit solvent molecule used in DFT calculations. [b] Experimental values are in parentheses.

coupling and via water nucleophilic attack. In all cases, when $Ru^V{=}O$ species were thermodynamically accessible via PCET, the presence of these species was verified by spectroscopy.[16,20,21,27] However, despite the assumed accessibility of the $[Ru^V{=}O(bpy)(EtO\text{-}tpy)]^{3+}$ state, the corresponding EPR was not detected (Figure 3B). Moreover, the calculated $Ru^V{=}O$ potentials for the three analyzed complexes (Table 1) do not correlate with the rate of O_2 evolution. At the same time, we noted that the onset of catalytic current (~1.6 V and ~1.4 V for **1** and **1-NO**; Figure 5C) happens at a potential higher than formation of the Ru^{IV} state. This was earlier interpreted as an indicator for Ru^{IV}-to-Ru^V oxidation.[28] However, it can also correspond to a ligand oxidation. For instance, the most oxidatively potent bioinorganic compound, Complex I, is known to contain an $Fe^{IV}{=}O$ unit and an oxidized ligand in a cation radical form.[60] The computed redox potentials for the ligand cation radicals listed in Table 1 correlate significantly better with O_2 evolution activity (Figure 6). Frontier orbitals (HOMO) of the $[Ru^{IV}{=}O]^{2+}$ states show delocalization onto EtO-tpy and bpy-NO ligands (Figure S10), suggesting that electron removal can happen from a ligand localized orbital or that oxidized species can have a multi-configurational character. Alternatively, ligands with lower oxidation potentials can acquire N-oxides more readily, causing an increase in catalytic activity. For complexes with bpy-NO, tpy-NO, and EtO-tpy-NO ligands, NO group de-coordination (i) opens the PCET channel via recruitment of the additional water ligand into the first coordination sphere of Ru; (ii) results in $[Ru^{IV}{=}O(ligandNO^{\bullet+})]$ states which carry three holes but are significantly more accessible (~1.5 V, Table 1) than $[Ru^V{=}O]^{3+}$ states (~2.0 eV); and (iii) have redox potential above the +1.23 V required for water oxidation. Thus, we can suggest that, if $Ru^V{=}O$ formation is prohibitively high thermodynamically (due to the lack of the PCET), the catalytically competent $[Ru^{IV}{=}O(\text{cation radical}^{+\bullet})]$ state might form, ensuring activity in the water oxidation. More experiments are underway to elucidate the pathway for O−O bond formation, and the results will be reported in a follow-up paper.

Overall, *de novo* synthesis and isolation of the reactive catalytic intermediate $[Ru(tpy)(bpy\text{-}NO)(H_2O)]^{2+}$ resulted in material with high catalytic potency. Thus, the mere presence of such an intermediate or similar tpy-NO in the reaction mixtures at a level of few percent can account for the entire catalytic activity of the most-studied $[(tpy)Ru(bpy)(H_2O)]^{2+}$ family of Ru-based water oxidation catalysts. A difference of 2 orders of magnitude in catalytic activity was correlated with the redox property of the ligand toward formation of the cation radical.

MATERIALS AND METHODS

Ultrapure nitric acid was used (Catalog No. 225711 from Sigma-Aldrich). Commercially available ligands and precursors were used, such as bpy, tpy, bpy-NO, and 4′-chloro-terpyridine. Aqueous solutions were prepared using ultrapure (Type 1) water (resistivity 18.2 MΩ·cm at 25 °C, TOC 4 μg/L), Millipore.

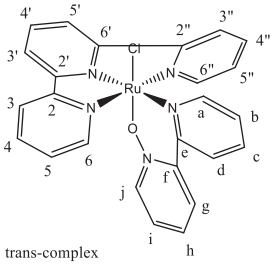

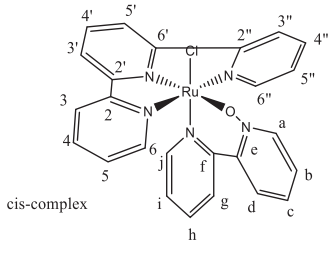

DOI: 10.1021/jacs.9b10265
J. Am. Chem. Soc. 2020, 142, 884−893

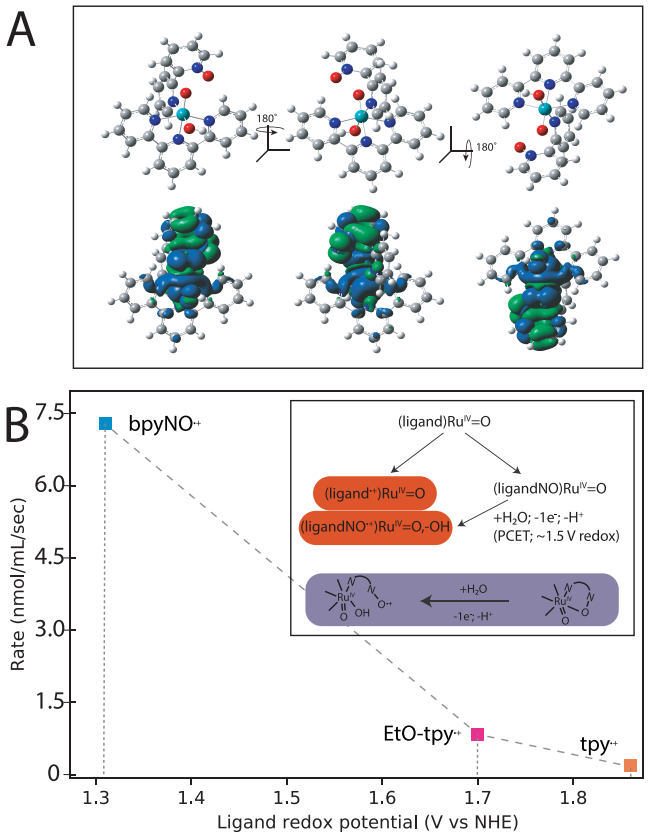

Figure 6. (A) Spin density of $[Ru^{IV}{=}O(tpy)(bpyNO^{\bullet+}{}_{out})(OH)]^{2+}$ in three different views. (B) DFT computed $Ru^{V}{=}O$ redox potentials (Table 1) do not correlate with the rate of O_2 evolution. We found that redox potentials for ligand oxidation (dashed lines) correlate better with O_2 evolution rates. Transient ligand oxidation with the formation of the ligand-N-oxide lowers the oxidation potential of the ligand, allowing it to store the third hole needed for water activation.

$[Ru^{II}(bpy)(tpy)Cl]Cl$ and $[Ru^{II}(bpy)(4'\text{-EtO-tpy})Cl]Cl$ (tpy = 2,2′;6′,2″-terpyridine, bpy = 2,2′-bipyridine) were synthesized and characterized as described in the literature.[32,58] The synthesis of the $[Ru(tpy)(C_2O_4)(H_2O)]\cdot 2H_2O$ reference compound was performed according to a procedure described previously.[61] bpy-NO ligand was obtained from Sigma-Aldrich. $[Ru(tpy)(bpy\text{-}NO)Cl]Cl$ was prepared by a procedure similar to the synthesis of the $[Ru^{II}(bpy)(tpy)Cl]Cl$,[61] with following details:

150 mg of $Ru(tpy)Cl_3$ (0.34 mmol), 58 mg of bpy-NO (1 equiv), 0.1 mL of trimethylamine, and 30 mg of LiCl were mixed in a solution of 40 mL of ethanol and 2 mL of water and refluxed for 1 h at a temperature not exceeding 100 °C. After cooling to room temperature, all solvents were evaporated at reduced pressure to dryness. ^{1}H NMR of a residue was taken, showing the presence of 61% of $[Ru(tpy)(bpy\text{-}NO)Cl]Cl$. The residue was separated using 100% ethanol on a silica gel column (Sorbtech, 200 × 400 mesh), collecting 3−4 mL fractions. Products in the fractions were monitored by UV−vis and NMR. All steps of the synthesis were completed under dim red light due to suspected light sensitivity. Elution from the silica gel column with ethanol resulted in first a purple fraction of *trans*- isomer with a very low content of compound; later $[Ru(bpy)(tpy)Cl]^+$ was eluted, followed by fractions enriched with *cis*-$[Ru(bpy\text{-}NO)(tpy)Cl]^+$. Later fractions allowed us to isolate pure *cis*-$Ru(bpyNO)(tpy)Cl_2$ for catalytic tests and spectroscopy.

^{1}H NMR (DMSO-d_6) of *cis*-$[Ru(bpyNO)(tpy)Cl]^+$ (Figure S11). δ 9.61 (d, 1H, Ha), 8.66−8.70 (dd, 4H, H3′/H5′, H3/H3″), 8.32 (d, 1H, Hd), 8.26 (d, 1H, Hg), 8.66 (d, 2H, H3/H3″), 8.15 (td, 1H, H4′), 8.05 (td, 2H, H4/H4″), 7.92−7.84 (m, 4H, Hb,Hc,H6/H6″), 7.78 (td, 1H, Hh), 7.54 (ddd, 2H, H5/H5″), 7.03 (ddd, 1H, Hi), 6.82 (d, 1H, Hj).

^{13}C NMR (DMSO-d_6) of *cis*-$[Ru(bpyNO)(tpy)Cl]^+$ (Figure S12). δ 160.34 (C2/C2″), 159.16 (C2′/C6′), 151.76 (Ce), 150.77 (Ca), 150.25 (C6/C6′), 146.96 (Cc), 143.71 (Cb), 137.42 (C4/C4″), 137.20 (Cd), 136.22 (C4′), 131.34 (Cf), 130.29 (Cj), 128.83 (Ch), 128.63 (Ci), 127.29 (C5/C5′), 126.91 (Cg), 123.82 (C3/C3″), 122.87 (C3′/C5′).

^{1}H NMR (DMSO-d_6) of *trans*-$[Ru(bpyNO)(tpy)Cl]^+$. δ 10.06 (d, 1H, Ha), 8.97 (d, 1H, Hd), 8.87 (d, 2H, H3′/H5′), 8.75 (d, 2H, H3/H3″), 8.72 (d, 1H, Hg), 8.36 (td, 1H, Hc), 8.20 (t, 1H, H4′), 8.06 (ddd, 1H, Hb), 7.96 (td, 2H, H4/H4″), 7.76 (td, 1H, Hh), 7.59 (d, 2H, H6/H6″), 7.38 (ddd, 2H, H5/H5″), 7.31 (d, 1H, Hj), 7.29 (ddd, 1H, Hi).

^{1}H NMR spectra were recorded on a Bruker AV500 spectrometer equipped with a 5 mm BBFO Z-gradient probe. All measurements were performed at room temperature. Chemical shifts were referenced to the residual solvent peak.

$[Ru^{II}(bpy)(tpy)(H_2O)]Cl_2$, $[Ru^{II}(bpy)(4'\text{-EtO-tpy})(H_2O)]Cl_2$, and $[Ru^{II}(bpy\text{-}NO)(tpy)(H_2O)]Cl_2$ were prepared by aging the corresponding chlorides in pure water for 24 h. After that, 2 equiv of silver nitrate was added to the solution, which then was filtered in order to remove Cl ions. When Ce^{IV} is used as the oxidant, it is prepared freshly daily. O_2 evolution activity using Ce^{IV} was in agreement with earlier reports.[18,32,36,62] Oxygen evolution was measured with a PC-operated Clark-type polarographic oxygen electrode from Oxygraph Systems (Hansatech Instruments Ltd.). The sample was housed within a hermetic borosilicate glass reaction vessel. Calibration was carried out by measurements of the signal from O_2-saturated water in an open reaction vessel. Sodium dithionite, an oxygen-depleting agent, was added to the water, and the drop in the signal was related to the solubility of oxygen in water at room temperature (262 μmol/L). The glass vessel was thoroughly washed with water, and 0.6 mL of Ru complex solution in 0.1 M HNO_3 was added. A defined number of Ce^{IV} equivalents were carefully added into the chamber, and oxygen evolution was measured as a function of time.

To prepare EPR samples, 200 μL of a 1 mM solution of Ru complex in 0.1 M HNO_3 were oxidized with a defined number of Ce^{IV} equivalents, transferred in an EPR tube, and frozen in liquid nitrogen within 30 s. Low-temperature X-band EPR spectra were recorded with a Bruker EMX X-band spectrometer equipped with an X-band CW microwave bridge. The sample temperature was maintained at 20 K using a ColdEdge closed cycle cryostat. For EPR signal quantitation, the standard EPR sample tubes were filled with sample through all of the resonator space, and signal intensities were measured on the same day and under the same conditions to allow direct comparison of the signal intensities.

The resonance Raman spectra were collected using a HeCd CW laser with a wavelength of 420 nm, 20 mW power, and a second-harmonic wave of Nd:YAG (532 nm). The sample was held in a Teflon custom-designed electrochemical cell with a clear polypropylene thin-film window for bulk electrolysis resonance Raman measurement. For the Ce^{IV} treatment, a drop of sample directly was exposed to laser light. The diameter of the laser beam at the sample was about 0.5 mm. The orientation of the laser beam, the sample, and the detector was held at 0°. Two fused silica lenses were used to collect the Raman signal and focus it at the Shamrock 303i spectrometer input slit. The slit width was 50 μm. The Semrock edge-pass filter eliminated the Rayleigh scattering to get into the spectrometer. Holographic gratings of 1800 l/mm for the 442 nm laser and 1200 l/mm (grating blaze 500) for the 532 nm laser were used to disperse the light and later collimated light exposed on iDus 420 Andor camera.

The DFT calculations were performed with Gaussian09 using the B3LYP exchange-correlation (XC) functional. The 6-31G* basis was set for all organic atoms (C, O, N, H), and the all-electron DGDZVP basis was set for the Ru atom. The CPCM polarizable conductor model was used to model water solvation. The value of the reference potential (NHE) was assigned as 4.44 V, and the solvation free energy

DOI: 10.1021/jacs.9b10265
J. Am. Chem. Soc. 2020, 142, 884−893

of a proton was −11.64 V. Results of DFT calculations are shown in Figures S6−S9 and in Tables S4−S7. Structures are given in Table S6. Earlier we demonstrated that this computational technique reproduces bond distances and redox potentials of the Ru complexes.[16−18,24,63] With our calculation protocol, we have achieved matches (within expected 0.2 eV) to all unambiguously known redox potentials for all Ru complexes as outlined in our earlier publications.[16−18]

A Thermo Nicolet Nexus FTIR spectrometer was used to conduct FTIR measurements. OMNIC software, a MCT detector, and a KBr beam splitter are some of specifications of the spectrometer. The spectrometer was continuously purged with nitrogen gas before and during measurements. For data collection, the powder sample was pressed against an attenuated total reflectance (ATR) diamond crystal. The measurement was conducted in the dark, at room temperature, and in dim ambient light to make sure the light does not cause unintended reactions. The graph consists of 36 scans with 4 cm^{-1} resolution.

UV−vis absorptions spectroscopy was conducted by using a Cary 300 UV−vis spectrometer. All solutions were measured in a quartz cuvette with a path line of 1 mm.

All of the electrochemistry experiments were conducted with a BASi Epsilon potentiostat with a platinum counter electrode and Ag/AgCl (saturated KCl) as the reference electrode. The reference electrode was calibrated against the $Fe(CN)_6^{3-}/Fe(CN)_6^{4-}$ redox couple in 0.5 *m* NaCl, which should be 0.208 V versus Ag/AgCl (saturated KCl). Bulk electrolysis experiments were performed in a three-compartment electrochemical cell, with each compartment separated by porous glass frits. For cyclic voltammetry, a polished platinum electrode with Ag/AgCl (saturated KCl) as reference electrode was used. The scan rate in CV was 0.1 V/s. All the solutions were in 0.1 M HNO_3, and all the presented measurements already have pure platinum and 0.1 M HNO_3 subtracted as background.

■ ASSOCIATED CONTENT

Supporting Information

The Supporting Information is available free of charge at https://pubs.acs.org/doi/10.1021/jacs.9b10265.

Additional literature overview for *g*-factors of Ru^V complexes, additional experimental data on NMR, resonance Raman and catalytic oxygen evolution of Ru complexes; summary of DFT energies, reactions energetics, DFT computed Latimer−Frost diagrams and visualization of HOMO orbitals for **1**, **2**, and **1-NO**, including Figures S1−S12 and Tables S1−S7 (PDF)

■ AUTHOR INFORMATION

Corresponding Author

*ypushkar@purdue.edu

ORCID

Alireza Karbakhsh Ravari: 0000-0003-4273-5673

Yulia Pushkar: 0000-0001-7949-6472

Notes

The authors declare no competing financial interest.

■ ACKNOWLEDGMENTS

This work was supported by the National Science Foundation, Division of Chemistry, CHE-1900476 (Y.P.). Access to EPR was provided by the Amy Instrumentation Facility, Department of Chemistry, under the supervision of Dr. Michael Everly. We thank Prof. L. Slipchenko and Dr. Mark Palenik for helpful discussion.

■ REFERENCES

(1) De Luna, P.; Hahn, C.; Higgins, D.; Jaffer, S. A.; Jaramillo, T. F.; Sargent, E. H. What would it take for renewably powered electrosynthesis to displace petrochemical processes? *Science* **2019**, *364* (6438), No. eaav3506.

(2) Suga, M.; Akita, F.; Sugahara, M.; Kubo, M.; Nakajima, Y.; Nakane, T.; Yamashita, K.; Umena, Y.; Nakabayashi, M.; Yamane, T.; Nakano, T.; Suzuki, M.; Masuda, T.; Inoue, S.; Kimura, T.; Nomura, T.; Yonekura, S.; Yu, L.-J.; Sakamoto, T.; Motomura, T.; Chen, J.-H.; Kato, Y.; Noguchi, T.; Tono, K.; Joti, Y.; Kameshima, T.; Hatsui, T.; Nango, E.; Tanaka, R.; Naitow, H.; Matsuura, Y.; Yamashita, A.; Yamamoto, M.; Nureki, O.; Yabashi, M.; Ishikawa, T.; Iwata, S.; Shen, J.-R. Light-induced structural changes and the site of O = O bond formation in PSII caught by XFEL. *Nature* **2017**, *543* (7643), 131−135.

(3) Kern, J.; Chatterjee, R.; Young, I. D.; Fuller, F. D.; Lassalle, L.; Ibrahim, M.; Gul, S.; Fransson, T.; Brewster, A. S.; Alonso-Mori, R.; Hussein, R.; Zhang, M.; Douthit, L.; de Lichtenberg, C.; Cheah, M. H.; Shevela, D.; Wersig, J.; Seuffert, I.; Sokaras, D.; Pastor, E.; Weninger, C.; Kroll, T.; Sierra, R. G.; Aller, P.; Butryn, A.; Orville, A. M.; Liang, M.; Batyuk, A.; Koglin, J. E.; Carbajo, S.; Boutet, S.; Moriarty, N. W.; Holton, J. M.; Dobbek, H.; Adams, P. D.; Bergmann, U.; Sauter, N. K.; Zouni, A.; Messinger, J.; Yano, J.; Yachandra, V. K. Structures of the intermediates of Kok's photosynthetic water oxidation clock. *Nature* **2018**, *563* (7731), 421−425.

(4) Davis, K. M.; Sullivan, B. T.; Palenik, M. C.; Yan, L.; Purohit, V.; Robison, G.; Kosheleva, I.; Henning, R. W.; Seidler, G. T.; Pushkar, Y. Rapid Evolution of the Photosystem II Electronic Structure during Water Splitting. *Phys. Rev. X* **2018**, *8* (4), 041014.

(5) Davis, K. M.; Pushkar, Y. N. Structure of the Oxygen Evolving Complex of Photosystem II at Room Temperature. *J. Phys. Chem. B* **2015**, *119* (8), 3492−3498.

(6) Davis, K. M.; Sullivan, B. T.; Palenik, M. C.; Yan, L.; Purohit, V.; Robison, G.; Kosheleva, I.; Henning, R. W.; Seidler, G. T.; Pushkar, Y. Rapid Evolution of the Photosystem II Electronic Structure During Water Splitting. *Phys. Rev. X* **2018**, *8*, 041014.

(7) Blakemore, J. D.; Crabtree, R. H.; Brudvig, G. W. Molecular Catalysts for Water Oxidation. *Chem. Rev.* **2015**, *115* (23), 12974−13005.

(8) House, R. L.; Iha, N. Y. M.; Coppo, R. L.; Alibabaei, L.; Sherman, B. D.; Kang, P.; Brennaman, M. K.; Hoertz, P. G.; Meyer, T. J. Artificial photosynthesis: Where are we now? Where can we go? *J. Photochem. Photobiol., C* **2015**, *25*, 32−45.

(9) Li, J.; Guttinger, R.; More, R.; Song, F.; Wan, W.; Patzke, G. R. Frontiers of water oxidation: the quest for true catalysts. *Chem. Soc. Rev.* **2017**, *46* (20), 6124−6147.

(10) Matheu, R.; Garrido-Barros, P.; Gil-Sepulcre, M.; Ertem, M. Z.; Sala, X.; Gimbert-Surinach, C.; Llobet, A. The development of molecular water oxidation catalysts. *Nat. Rev. Chem.* **2019**, *3* (5), 331−341.

(11) Pushkar, Y.; Davis, K. M.; Palenik, M. Model of the Oxygen Evolving Complex Which is Highly Predisposed to O−O Bond Formation. *J. Phys. Chem. Lett.* **2018**, *9*, 3525−3531.

(12) Pushkar, Y.; Ravari, A. K.; Jensen, S. C.; Palenik, M. Early Binding of Substrate Oxygen Is Responsible for a Spectroscopically Distinct S2 State in Photosystem II. *J. Phys. Chem. Lett.* **2019**, *10* (17), 5284−5291.

(13) Ye, S.; Ding, C.; Liu, M.; Wang, A.; Huang, Q.; Li, C. Water Oxidation Catalysts for Artificial Photosynthesis. *Adv. Mater.* **2019**, *31* (50), 1902069.

(14) Zhang, B.; Sun, L. Artificial photosynthesis: opportunities and challenges of molecular catalysts. *Chem. Soc. Rev.* **2019**, *48* (7), 2216−2264.

(15) Garrido-Barros, P.; Gimbert-Surinach, C.; Matheu, R.; Sala, X.; Llobet, A. How to make an efficient and robust molecular catalyst for water oxidation. *Chem. Soc. Rev.* **2017**, *46* (20), 6088−6098.

(16) Lebedev, D.; Pineda-Galvan, Y.; Tokimaru, Y.; Fedorov, A.; Kaeffer, N.; Copéret, C.; Pushkar, Y. The Key Ru^V = O Intermediate of Site-Isolated Mononuclear Water Oxidation Catalyst Detected by

DOI: 10.1021/jacs.9b10265
J. Am. Chem. Soc. 2020, 142, 884−893

in Situ X-ray Absorption Spectroscopy. *J. Am. Chem. Soc.* **2018**, *140* (1), 451−458.
(17) Moonshiram, D.; Pineda-Galvan, Y.; Erdman, D.; Palenik, M.; Zong, R. F.; Thummel, R.; Pushkar, Y. Uncovering the Role of Oxygen Atom Transfer in Ru-Based Catalytic Water Oxidation. *J. Am. Chem. Soc.* **2016**, *138* (48), 15605−15616.
(18) Pushkar, Y.; Moonshiram, D.; Purohit, V.; Yan, L.; Alperovich, I. Spectroscopic Analysis of Catalytic Water Oxidation by [Ru^{II}(bpy)-(tpy)H_2O]2+ Suggests That Ru^{V} = O Is Not a Rate-Limiting Intermediate. *J. Am. Chem. Soc.* **2014**, *136* (34), 11938−11945.
(19) Gersten, S. W.; Samuels, G. J.; Meyer, T. J. Catalytic oxidation of water by an oxo-bridged ruthenium dimer. *J. Am. Chem. Soc.* **1982**, *104* (14), 4029−4030.
(20) Moonshiram, D.; Alperovich, I.; Concepcion, J. J.; Meyer, T. J.; Pushkar, Y. Experimental demonstration of radicaloid character in a Ru-V = O intermediate in catalytic water oxidation. *Proc. Natl. Acad. Sci. U. S. A.* **2013**, *110* (10), 3765−3770.
(21) Moonshiram, D.; Jurss, J. W.; Concepcion, J. J.; Zakharova, T.; Alperovich, I.; Meyer, T. J.; Pushkar, Y. Structure and electronic configurations of the intermediates of water oxidation in blue ruthenium dimer catalysis. *J. Am. Chem. Soc.* **2012**, *134* (10), 4625−36.
(22) Stull, J. A.; Britt, R. D.; McHale, J. L.; Knorr, F. J.; Lymar, S. V.; Hurst, J. K. Anomalous reactivity of ceric nitrate in ruthenium "blue dimer"-catalyzed water oxidation. *J. Am. Chem. Soc.* **2012**, *134* (49), 19973−6.
(23) Planas, N.; Vigara, L.; Cady, C.; Miro, P.; Huang, P.; Hammarstrom, L.; Styring, S.; Leidel, N.; Dau, H.; Haumann, M.; Gagliardi, L.; Cramer, C. J.; Llobet, A. Electronic Structure of Oxidized Complexes Derived from cis-Ru(II)(bpy)(2)(H(2)O)(2)](2+) and Its Photoisomerization Mechanism. *Inorg. Chem.* **2011**, *50* (21), 11134−11142.
(24) Erdman, D.; Pineda-Galvan, Y.; Pushkar, Y. Mechanistic Analysis of Water Oxidation Catalyst cis- Ru(bpy)(2)(H2O)(2)(2+): Effect of Dimerization. *Catalysts* **2017**, *7* (12), 39.
(25) Duan, L. L.; Bozoglian, F.; Mandal, S.; Stewart, B.; Privalov, T.; Llobet, A.; Sun, L. C. A molecular ruthenium catalyst with water-oxidation activity comparable to that of photosystem II. *Nat. Chem.* **2012**, *4* (5), 418−423.
(26) Duan, L. L.; Araujo, C. M.; Ahlquist, M. S. G.; Sun, L. C. Highly efficient and robust molecular ruthenium catalysts for water oxidation. *Proc. Natl. Acad. Sci. U. S. A.* **2012**, *109* (39), 15584−15588.
(27) Pineda-Galvan, Y.; Ravari, A. K.; Shmakov, S.; Lifshits, L.; Kaveevivitchai, N.; Thummel, R.; Pushkar, Y. Detection of the site protected 7-coordinate Ru^{V} = O species and its chemical reactivity to enable catalytic water oxidation. *J. Catal.* **2019**, *375*, 1−7.
(28) Wasylenko, D. J.; Ganesamoorthy, C.; Henderson, M. A.; Koivisto, B. D.; Osthoff, H. D.; Berlinguette, C. P. Electronic Modification of the [Ru-II(tpy)(bpy)(OH2)](2+) Scaffold: Effects on Catalytic Water Oxidation. *J. Am. Chem. Soc.* **2010**, *132* (45), 16094−16106.
(29) Marelius, D. C.; Bhagan, S.; Charboneau, D. J.; Schroeder, K. M.; Kamdar, J. M.; McGettigan, A. R.; Freeman, B. J.; Moore, C. E.; Rheingold, A. L.; Cooksy, A. L.; Smith, D. K.; Paul, J. J.; Papish, E. T.; Grotjahn, D. B. How Do Proximal Hydroxy or Methoxy Groups on the Bidentate Ligand Affect (2,2';6',2''-Terpyridine)Ru-(N,N)X Water-Oxidation Catalysts? Synthesis, Characterization, and Reactivity at Acidic and Near-Neutral pH. *Eur. J. Inorg. Chem.* **2014**, *4*, 676−689.
(30) Maji, S.; Lopez, I.; Bozoglian, F.; Benet-Buchholz, J.; Llobet, A. Mononuclear Ruthenium-Water Oxidation Catalysts: Discerning between Electronic and Hydrogen-Bonding Effects. *Inorg. Chem.* **2013**, *52* (7), 3591−3593.
(31) Yoshida, M.; Kondo, M.; Torii, S.; Sakai, K.; Masaoka, S. Oxygen Evolution Catalyzed by a Mononuclear Ruthenium Complex Bearing Pendant SO3− Groups. *Angew. Chem.* **2015**, *127* (27), 8092−8095.
(32) Yagi, M.; Tajima, S.; Komi, M.; Yamazaki, H. Highly active and tunable catalysts for O-2 evolution from water based on mononuclear ruthenium(II) monoaquo complexes. *Dalton Trans.* **2011**, *40* (15), 3802−3804.
(33) Honta, J.; Tajima, S.; Sato, T.; Saito, K.; Yui, T.; Yagi, M. Spectroelectrochemical investigation of electrocatalytic water oxidation by a mononuclear ruthenium complex in a homogeneous solution. *J. Photochem. Photobiol., A* **2015**, *313*, 126−130.
(34) Lin, S.; Pineda-Galvan, Y.; Maza, W. A.; Epley, C. C.; Zhu, J.; Kessinger, M. C.; Pushkar, Y.; Morris, A. J. Electrochemical Water Oxidation by a Catalyst-Modified Metal−Organic Framework Thin Film. *ChemSusChem* **2017**, *10* (3), 514−522.
(35) Brennaman, M. K.; Gish, M. K.; Alibabaei, L.; Norris, M. R.; Binstead, R. A.; Nayak, A.; Lapides, A. M.; Song, W. J.; Brown, R. J.; Concepcion, J. J.; Templeton, J. L.; Papanikolas, J. M.; Meyer, T. J. Pathways Following Electron Injection: Medium Effects and Cross-Surface Electron Transfer in a Ruthenium-Based, Chromophore-Catalyst Assembly on TiO2. *J. Phys. Chem. C* **2018**, *122* (24), 13017−13026.
(36) Masaoka, S.; Sakai, K. Clear Evidence Showing the Robustness of a Highly Active Oxygen-evolving Mononuclear Ruthenium Complex with an Aqua Ligand. *Chem. Lett.* **2009**, *38* (2), 182−183.
(37) Concepcion, J. J.; Tsai, M. K.; Muckerman, J. T.; Meyer, T. J. Mechanism of Water Oxidation by Single-Site Ruthenium Complex Catalysts. *J. Am. Chem. Soc.* **2010**, *132* (5), 1545−1557.
(38) Yan, L. F.; Zong, R. F.; Pushkar, Y. Unexpected ligand lability in condition of water oxidation catalysis. *J. Catal.* **2015**, *330*, 255−260.
(39) Hughes, T. F.; Friesner, R. A. Systematic Investigation of the Catalytic Cycle of a Single Site Ruthenium Oxygen Evolving Complex Using Density Functional Theory. *J. Phys. Chem. B* **2011**, *115* (29), 9280−9289.
(40) Sala, X.; Ertem, M. Z.; Vigara, L.; Todorova, T. K.; Chen, W. Z.; Rocha, R. C.; Aquilante, F.; Cramer, C. J.; Gagliardi, L.; Llobet, A. The cis-[Ru-II(bpy)(2)(H_2O)(2)](2+) Water-Oxidation Catalyst Revisited. *Angew. Chem., Int. Ed.* **2010**, *49* (42), 7745−7747.
(41) Vigara, L.; Ertem, M. Z.; Planas, N.; Bozoglian, F.; Leidel, N.; Dau, H.; Haumann, M.; Gagliardi, L.; Cramer, C. J.; Llobet, A. Experimental and quantum chemical characterization of the water oxidation cycle catalysed by [Ru-II(damp)(bpy)(H_2O)](2+). *Chem. Sci.* **2012**, *3* (8), 2576−2586.
(42) Privalov, T.; Akermark, B.; Sun, L. C. The O-O Bonding in Water Oxidation: the Electronic Structure Portrayal of a Concerted Oxygen Atom-Proton Transfer Pathway. *Chem. - Eur. J.* **2011**, *17* (30), 8313−8317.
(43) Angeles-Boza, A. M.; Ertem, M. Z.; Sarma, R.; Ibanez, C. H.; Maji, S.; Llobet, A.; Cramer, C. J.; Roth, J. P. Competitive oxygen-18 kinetic isotope effects expose O-O bond formation in water oxidation catalysis by monomeric and dimeric ruthenium complexes. *Chem. Sci.* **2014**, *5* (3), 1141−1152.
(44) Tong, L. P.; Inge, A. K.; Duan, L. L.; Wang, L.; Zou, X. D.; Sun, L. C. Catalytic Water Oxidation by Mononuclear Ru Complexes with an Anionic Ancillary Ligand. *Inorg. Chem.* **2013**, *52* (5), 2505−2518.
(45) Kimoto, A.; Yamauchi, K.; Yoshida, M.; Masaoka, S.; Sakai, K. Kinetics and DFT studies on water oxidation by Ce4+ catalyzed by [Ru(terpy)(bpy)(OH2)]2+. *Chem. Commun.* **2012**, *48* (2), 239−41.
(46) Karmalkar, D. G.; Sankaralingam, M.; Seo, M. S.; Ezhov, R.; Lee, Y. M.; Pushkar, Y. N.; Kim, W. S.; Fukuzumi, S.; Nam, W. A High-Valent Manganese(IV)-Oxo-Cerium(IV) Complex and Its Enhanced Oxidizing Reactivity. *Angew. Chem., Int. Ed.* **2019**, *58*, 16124−16129.
(47) Liu, Y. Y.; Ng, S. M.; Yiu, S. M.; Lam, W. W. Y.; Wei, X. G.; Lau, K. C.; Lau, T. C. Catalytic Water Oxidation by Ruthenium(II) Quaterpyridine (qpy) Complexes: Evidence for Ruthenium(III) qpy-N,N"'-dioxide as the Real Catalysts. *Angew. Chem., Int. Ed.* **2014**, *53* (52), 14468−14471.
(48) Wang, Y.; Rinkevicius, Z.; Ahlquist, M. S. G. Formation of N-oxide in the third oxidation of Ru-II(tpy)(L)(OH2) (2+). *Chem. Commun.* **2017**, *53* (41), 5622−5624.

DOI: 10.1021/jacs.9b10265
J. Am. Chem. Soc. 2020, 142, 884−893

(49) Raynor, J. B.; Jeliazkowa, B. G. Electron-Spin Resonance-Spectra of Some Low-Spin Ruthenium(III) Complexes - A Probe for Solvation Effects. *J. Chem. Soc., Dalton Trans.* **1982**, *7*, 1185−1189.
(50) Dengel, A. C.; Griffith, W. P. Studies on transition-metal oxo and nitrido complexes. 12. Synthesis, spectroscopic properties, and reactions of stable ruthenium(V) and osmium(V) oxo complexes containing.alpha.-hydroxy carboxylate and.alpha.-amino carboxylate ligands. *Inorg. Chem.* **1991**, *30* (4), 869−871.
(51) Lin, S. Y.; Ravari, A. K.; Zhu, J.; Usov, P. M.; Cai, M.; Ahrenholtz, S. R.; Pushkar, Y.; Morris, A. J. Insight into Metal-Organic Framework Reactivity: Chemical Water Oxidation Catalyzed by a Ru(tpy)(dcbpy)(OH2) (2+)-Modified UiO-67. *ChemSusChem* **2018**, *11* (2), 464−471.
(52) Keidel, A.; López, I.; Staffa, J.; Kuhlmann, U.; Bozoglian, F.; Gimbert-Suriñach, C.; Benet-Buchholz, J.; Hildebrandt, P.; Llobet, A. Electrochemical and Resonance Raman Spectroscopic Studies of Water-Oxidizing Ruthenium Terpyridyl−Bipyridyl Complexes. *ChemSusChem* **2017**, *10* (3), 551−561.
(53) Pushkar, Y.; Pineda-Galvan, Y.; Ravari, A. K.; Otroshchenko, T.; Hartzler, D. A. Mechanism for O-O bond formation via radical coupling of metal and ligand based radicals − a new pathway. *J. Am. Chem. Soc.* **2018**, *140* (42), 13538−13541.
(54) Lopez, I.; Ertem, M. Z.; Maji, S.; Benet-Buchholz, J.; Keidel, A.; Kuhlmann, U.; Hildebrandt, P.; Cramer, C. J.; Batista, V. S.; Llobet, A. A Self-Improved Water-Oxidation Catalyst: Is One Site Really Enough? *Angew. Chem., Int. Ed.* **2014**, *53* (1), 205−209.
(55) Lopez, I.; Maji, S.; Benet-Buchholz, J.; Llobet, A. Oxo-Bridge Scenario behind Single-Site Water-Oxidation Catalysts. *Inorg. Chem.* **2015**, *54* (2), 658−666.
(56) Ghosh, P. K.; Brunschwig, B. S.; Chou, M.; Creutz, C.; Sutin, N. Thermal and Light-Induced Reduction of $Ru(BPY)_3(3+)$ in Aqueous-Solution. *J. Am. Chem. Soc.* **1984**, *106* (17), 4772−4783.
(57) Kojima, T.; Nakayama, K.; Sakaguchi, M.; Ogura, T.; Ohkubo, K.; Fukuzumi, S. Photochemical Activation of Ruthenium(II)-Pyridylamine Complexes Having a Pyridine-N-Oxide Pendant toward Oxygenation of Organic Substrates. *J. Am. Chem. Soc.* **2011**, *133* (44), 17901−17911.
(58) Takeuchi, K. J.; Thompson, M. S.; Pipes, D. W.; Meyer, T. J. Redox and spectral properties of monooxo polypyridyl complexes of ruthenium and osmium in aqueous media. *Inorg. Chem.* **1984**, *23* (13), 1845−1851.
(59) Matheu, R.; Ertem, M. Z.; Gimbert-Suriñach, C.; Sala, X.; Llobet, A. Seven Coordinated Molecular Ruthenium−Water Oxidation Catalysts: A Coordination Chemistry Journey. *Chem. Rev.* **2019**, *119* (6), 3453−3471.
(60) Rittle, J.; Green, M. T. Cytochrome P450 Compound I: Capture, Characterization, and C-H Bond Activation Kinetics. *Science* **2010**, *330* (6006), 933−937.
(61) Adeyemi, S. A.; Dovletoglou, A.; Guadalupe, A. R.; Meyer, T. J. Redox and Spectral Properties of the 4-Electron Oxidant trans-$Ru(TPY)(O)_2(H_2O)$ $(ClO_4)_2$. *Inorg. Chem.* **1992**, *31* (8), 1375−1383.
(62) Tseng, H. W.; Zong, R.; Muckerman, J. T.; Thummel, R. Mononuclear Ruthenium(II) Complexes That Catalyze Water Oxidation. *Inorg. Chem.* **2008**, *47* (24), 11763−11773.
(63) Moonshiram, D.; Purohit, V.; Concepcion, J. J.; Meyer, T. J.; Pushkar, Y. Mechanism of Catalytic Water Oxidation by the Ruthenium Blue Dimer Catalyst: Comparative Study in D2O versus H_2O. *Materials* **2013**, *6* (2), 392−409.

DOI: 10.1021/jacs.9b10265
J. Am. Chem. Soc. 2020, 142, 884−893